

Incommensurate spin and orbital magnetism of Mn atomic chains on W(110) surface

M. M. Bezerra-Neto¹, Y. O. Kvashnin², A. Bergman², R. B. Muniz³, O. Eriksson^{2,4}, M. I. Katsnelson⁵, and A. B. Klautau⁶

¹*Instituto de Engenharia e Geociências, Universidade Federal do Oeste do Pará, Santarém, PA, Brazil*

²*Department of Physics and Astronomy, Division of Materials Theory, Uppsala University, Box 516, SE-751 20, Sweden*

³*Instituto de Física, Universidade Federal Fluminense, 24210-346 Niterói, Rio de Janeiro, Brazil*

⁴*School of Science and Technology, Örebro University, SE-701 82, Örebro, Sweden*

⁵*Institute for Molecules and Materials, Radboud University, Heijendaalseweg 135, 6525AJ, Nijmegen, Netherlands and*

⁶*Faculdade de Física, Universidade Federal do Pará, Belém, PA, Brazil*

(Dated: August 21, 2021)

Stabilization of unusual spin-orbit driven magnetic orderings are achieved for chains of Mn atoms deposited on a W(110) substrate. First-principles electronic structure calculations show that the ground state spin configuration is non-collinear, forming spirals as a result of a competition between nearest and next-nearest neighbour exchange interactions. The orbital magnetic moments are also found to exhibit non-collinear ordering, that interestingly for some systems is incommensurate with the spin arrangement. We attribute such an exotic behaviour to the competition between the and spin-orbital interaction and crystal-field splitting effects. Model calculations based on this assumption reproduce the main findings observed in the first-principles calculations.

INTRODUCTION

Chiral spin textures, such as skyrmions [1, 2] and spin spirals [3–6], have attracted intense interest not only because of the fundamental physics governing their origins but also due to their potential applications in novel information storage technologies. Ultrathin magnetic films deposited on heavy metal substrates are good candidates for displaying complex spin textures. In general, the chiral spin states observed in these systems are induced by an interplay between the Dzyaloshinskii-Moriya (DM) interaction [7, 8], the bi-linear Heisenberg exchange interaction, and the magnetocrystalline anisotropy. Ultrathin layers of Mn/W(110) [3, 4] are one of these cases, where a combination of the relatively strong spin-orbit interaction of tungsten and the broken inversion symmetry at the interfaces lead to a significant interface-induced DM interaction. As a result, the ground-state spin magnetic moments display different types of spin spirals, depending on the number of Mn atomic planes. For a single Mn overlayer on W(110) the spin magnetic moments exhibit a cycloidal magnetic order as observed in Ref. 4. The Mn bilayer show a conical spin-spiral state along the [001] direction [3] and in both cases a unique rotational sense is enforced by the chiral DM interaction.

With the advent of *spin-orbitronics*, which seeks to explore phenomena intrinsically related to the spin-orbit coupling, the development of model Hamiltonians has gained momentum in recent years, and some new approaches have been discussed in the literature [9–13]. In this scenario, orbital moments became a focus of studies and have been explored in various aspects, such as: in the so-called orbital Hall effect, where an external electric field induces an orbital angular momentum current

that flows in the transverse direction of the applied field [14–16], in magnons that besides their spin magnetic moment may also carry orbital magnetic moment [17], as a means to exert torque in magnetic units [18], in the formation of Rashba-type surface band splittings that may lead to chiral orbital angular momentum states [19, 20], as well as in the connection between the anisotropy of the orbital magnetic moment and the DM interaction [21], among others. A model Hamiltonian based on realistic electronic structure that takes into account in a general way all relevant interactions remains a considerable challenge. One of the promising approaches is based on the consideration of small rotations near a given magnetic configuration (“magnetic force theorem”) as was previously suggested for purely spin rotations [22, 23]. Its generalization for the systems with unquenched orbital moments [9, 24] allows to write explicit formulas for spin-spin, orbital-orbital, and spin-orbital interactions but until now they were not applied to specific real materials.

Here, by means of first-principles calculations, we demonstrate the occurrence of atomic scale spin spirals in Mn chains placed on top of a W(110) surface. The choice of these systems was motivated by the remarkable magnetic properties observed for Mn overlayers on W(110) [3, 4], as well as by the possibility of fabricating atomic chains of transition metal atoms on heavy metal substrates. We have examined the ground state spin and orbital magnetic configurations of chains and nanoribbons (stripes) of Mn deposited along two distinct crystallographic directions of a W(110) surface. We found that the ground-state spin configuration of the Mn nanostructure changes with the increase of its width. The mono-atomic Mn chain display a spin spiral with helical nature, whereas Mn ribbons with three atoms in width

show a cycloidal spin spiral state. Such chiral magnetic orders are also revealed for the orbital moments in some cases, and depending on the length and width of the Mn nanostructures, the spin and orbital spiral configurations may exhibit different periods. We discuss the obtained magnetic chirality in terms of effective low energy Hamiltonians that contain spin-spin, orbital-orbital as well as spin-orbital exchange. The exotic behaviour concerning the incommensurate orbital spiral configurations with respect to the spin arrangement is microscopically attributed to a competition between crystal field and spin-orbit coupling, which are comparable in this material. Our model calculations, based on this assumption, reproduce the main findings observed in the first-principles calculations.

COMPUTATIONAL DETAILS

The density functional theory based calculations were performed using the first principles real-space linear muffin-tin orbital method within the atomic sphere approximation (RS-LMTO-ASA) [25–34], which has been generalized to treat non-collinear magnetism [13, 32, 35]. This method is based on the LMTO-ASA formalism [36] and employs the recursion method [37] to solve the eigenvalue problem directly in real space. All calculations are fully self-consistent and exchange-correlation effects were taken into account within the local spin density approximation (LSDA) [38]. We included the spin-orbit coupling term $\lambda \mathbf{L} \cdot \mathbf{S}$ self-consistently at each variational step, where \mathbf{L} and \mathbf{S} represent the orbital and spin angular momentum operators, and λ is the calculated spin-orbit coupling strength [39, 40].

We have considered Mn nanostructures, with different geometries, supported on a W(110) surface. The W(110) substrate is modeled by a cluster containing approximately 8000 atoms positioned in a bcc lattice with the experimental lattice parameter of W. In order to simulate the vacuum outside the bcc surface and to treat charge transfers correctly, we included two overlayers of empty spheres above the W surface. The calculations of the Mn adsorbed nanochains have been performed by embedding the clusters as a perturbation on the previously self-consistently converged W(110) surface. In order to achieve an accurate description of the hybridization with the substrate, the Mn sites and the closest shells of neighboring atoms (or empty spheres) around the Mn nanostructures were recalculated self-consistently. The continued fraction in the recursion method was appended with the Beer-Pettifor terminator [41] after 30 recursion levels.

The Heisenberg bi-linear exchange interactions J_{ij} and the DM vectors \vec{D}_{ij} were calculated with the use of the Liechtenstein–Katsnelson–Antropov–Gubanov (LKAG) formula [22, 23], as implemented in the RS-LMTO-ASA method [13, 35, 42–44]. Both J_{ij} and D_{ij}

have been obtained from the ferromagnetic configuration of the nanoclusters. Their values are then used to analyze the spin magnetic orderings explored in the full non-collinear calculations.

RESULTS AND DISCUSSIONS

Fig. 1 illustrates the finite Mn nanostructures adsorbed on W(110) that were investigated here. First, the ground-state spin magnetic configuration of these nanostructures was investigated and, subsequently, focus was put on their orbital magnetic orderings. We start the discussion with the mono-atomic chain (hereafter identified as NW, for nanowire) comprising of 15 Mn atoms deposited along the $[1\bar{1}1]$ direction, having 3.8 nm in length. Next, we focus on a double nanowire (DNW), constituted of two 9 atom long Mn chains, also placed along the $[1\bar{1}1]$ direction, with a length of 2.2 nm. Finally, two finite stripes with three Mn atoms in width, laid down along the $[1\bar{1}0]$ direction with lengths of 3.58 nm (Stripe1) and 7.17 nm (Stripe2), were examined. It should be noted that the spin magnetic moments of the Mn atoms quite generally depend upon the number of nearest neighbors. Fewer neighbors yield higher spin magnetic moments, with values ranging from $3.98\mu_B/\text{atom}$, for atoms located at the NW edges, to $3.08\mu_B/\text{atom}$ for the most central Mn site on Stripe2. It is also found here that the Mn atoms induce a relatively small spin polarization on the W atoms adjacent to the Mn nanostructures, with values $\approx 0.20\mu_B/\text{atom}$.

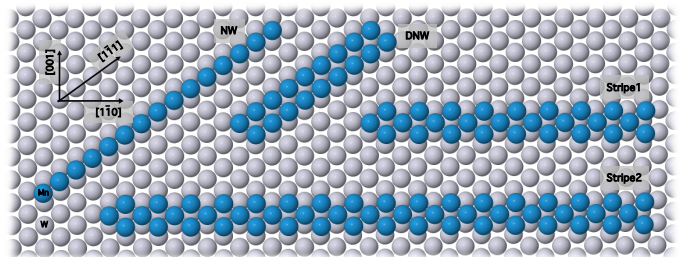


FIG. 1. (Color online) Mn nanostructures adsorbed on a W(110) surface: linear nanowire (NW), double nanowires (DNW), nanostripes (Stripe1 and Stripe2). The blue (dark) and gray (light) balls indicate Mn and W atoms, respectively.

Fig. 2 displays the non-collinear ground-state magnetic spin configurations calculated self-consistently for the nanostructures described above. The ground state spin moments of the NW exhibits an (*ortho*) helical-spin-spiral along the $[1\bar{1}1]$ direction, with a periodicity of ≈ 1.1 nm. The angles between spin magnetic moments of nearest neighbors (NN) Mn atoms is $\approx 90^\circ$ and the spin chirality is clock-wise. The DNW system presents a complex non-collinear configuration in which the spin magnetic moments of NN Mn atoms in different rows

are almost parallel, whereas among those located on the same row it is $\approx 135^\circ$. The first-principles calculations for the nanostructures reveal cycloidal spin spiral ground states, with long-range modulations along the $[1\bar{1}0]$ direction. Stripes 1 and 2 display half-periods of ≈ 3.6 nm and ≈ 7.24 nm, respectively, and inter-row antiferromagnetic ordering. These spin configurations resemble the ones observed by spin-polarized scanning tunneling microscopy measurements in a monolayer of Mn/W(110), which display a spin-spiral period of ≈ 6 nm propagating along the $[1\bar{1}0]$ direction [4].

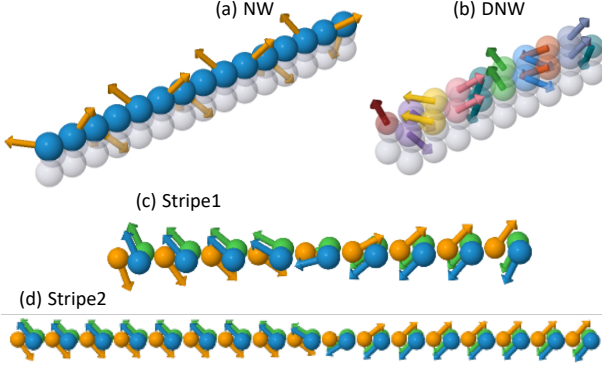


FIG. 2. Non-collinear ground-state spin magnetic configurations (moments shown by arrows) for Mn nanostructures adsorbed on a W(110) surface. (a) Nanowire (NW) with 15 Mn atoms; (b) Double nanowire (DNW) with 9 Mn atoms in length; (c) Stripe1 with 3 Mn atoms in breadth and 9 Mn atoms in length; (d) Stripe2 with 3 Mn atoms in breadth and 17 Mn atoms in length.

The calculated Heisenberg exchange interactions and the modulus of the DM vectors for the Mn nanostructures are shown in Fig. 3 for several pairs of Mn atoms as functions of their interatomic distances. We have only included the values for pairs of Mn atoms located around the center of the nanostructures. Those referring to atoms near the ends of the nanostructures' axes do not differ significantly from the ones shown in the figure and follow essentially the same qualitative trends. We note that $|J_{ij}|$ is larger for nearest neighbors Mn atoms and decreases relatively fast with the inter atomic distance. The trend of the distance dependence of the $|J_{ij}|$ parameters is also seen to be similar for all systems investigated here (Fig. 3a). It should also be noted that positive (negative) values of J_{ij} between the magnetic moments located at sites i and j represent a tendency for ferromagnetic (anti-ferromagnetic) alignment.

As shown in Fig. 3(b) the DM strength ($|\vec{D}_{ij}|$) between Mn NN pairs is smaller than the NN Heisenberg exchange interaction, and analogously for further neighbors. The DM vectors for all pairs of Mn atoms in the NW are along the $[001]$ direction. They are all in the plane, forming an angle of $\approx 54^\circ$ with the chain direction. Since the exchange interaction between NN Mn

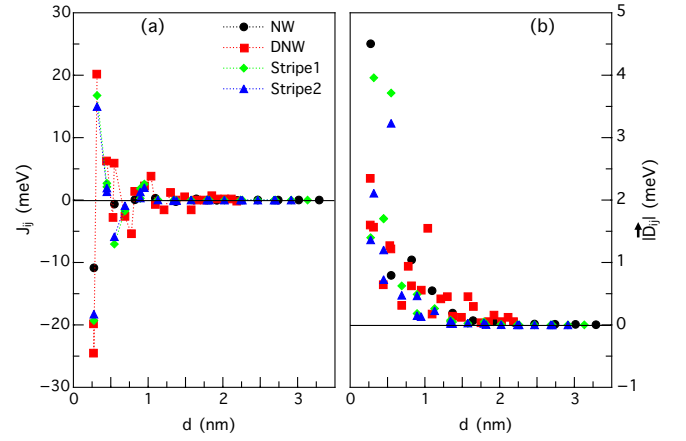


FIG. 3. The bi-linear Heisenberg exchange (J_{ij}) (a) and the Dzyaloshinskii-Moriya strengths ($|\vec{D}_{ij}|$) (b) interactions calculated for the Mn nanostructures in their ferromagnetic configurations. The interactions between Mn atoms around the nanostructure central regions are plotted as functions of the inter atomic Mn distances: black circles refer to the nanowire (NW); red squares are for the double-nanowire (DNW); green diamonds stand for the Stripe1 and blue triangles for Stripe2.

atoms is antiferromagnetic, in order to determine the magnetic anisotropy for the NW, we also performed self-consistent calculations considering a collinear ordering, and the magnetic anisotropy energy (MAE) for the NW was obtained by calculating the energy difference (ΔE) between the cases where the Mn moments are perpendicular to the plane (E_\perp) and in-plane (E_\parallel) along the wire direction. We obtained $\Delta E = E_\perp - E_\parallel \approx 1\text{meV}$, indicating that the easy axis is along the $[1\bar{1}1]$ direction (in the plane). The MAE in the presently investigated systems is therefore smaller than the NN DM and Heisenberg interactions, which represents a rather typical situation. The interplay between the J_{ij} and $|\vec{D}_{ij}|$ explains the helical spin-spiral obtained for the ground state magnetic configuration of the NW.

It is clear from Fig. 3 that the exchange interactions for the DNW, Stripe1 and Stripe2 nanostructures, have finite, but significant range, and is oscillatory. The DM vectors for the DNW are in-plane and they all point along the $[001]$ direction. The modulus of the DM vectors is also finite-ranged. The non-collinear spin textures shown in Fig. 2 can be explained from a competition between the DM and the bilinear exchange interactions. Concerning the stripes (Stripe1 and Stripe 2), the calculated chiral order of the spin-moments can be understood from the directions of the DM vectors, which point along the $[001]$ direction, leading to a tendency towards the formation of a cycloidal spin-spiral state that is propagating along the $[1\bar{1}0]$ direction (which is the stripes axes, see Fig. 1). Moreover, the periods of these spin-spirals are rather sensitive to changes in the $|\vec{D}_{ij}|$ values, since they are rather similar to the J_{ij} parameters, in both systems (see

Fig. 3).

Let us now turn our attention to the ground state orbital magnetic moment configurations of these nanostructures. The calculated orbital moments are depicted by red arrows in Fig. 4. The magnitude of the Mn orbital magnetic moments is $\approx 0.15\mu_B/\text{atom}$, whereas for the W atoms it is much smaller $\approx 0.005\mu_B/\text{atom}$. One may note that the local spin and orbital magnetic moments of each Mn atom in general are not collinear, as Fig. 4 illustrates. For the NW the orbital and spin moments are at

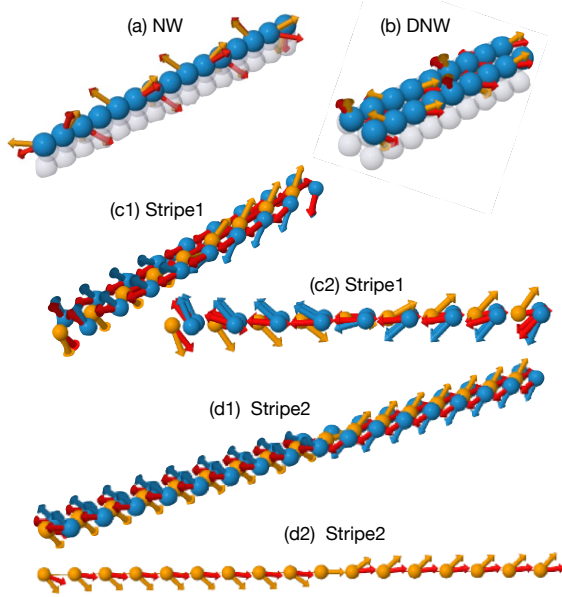


FIG. 4. (Color online) The spin and orbital ground state magnetic orderings calculated for Mn nanostructures adsorbed on a W(110) surface: (a) Mn nanowire (NW); (b) double nanowire (DNW), (c1-c2) top and lateral views of Stripe1, and (d1) Stripe2. (d2) Moments directions for only one row of the Stripe2 system. Yellow and blue arrows represent the directions of the local spin magnetic moment and the red arrows symbolize the corresponding orbital magnetic moment orientations.

an angle on each Mn site, but they present very similar spiral patterns, i.e. they have the same periodicity. In the case of the DNW, the spin and orbital magnetic configurations also have similar periodicity. However, in case of the stripes, the orbital moments have a distinct magnetic configuration, which is drastically different from, and incommensurate with, the spin arrangement. Except for the edge atoms, the orbital magnetic moments tend to align in-plane along the stripe's direction, both for Stripe1 and Stripe2.

In order to analyse the role played by the spin-orbit coupling on the ground state spin and orbital magnetic configurations, we have explored how the spin- and orbital moments vary for different values of the spin-orbit coupling strength (λ). In Fig. 5 we show results of the NW ground state spin and orbital magnetic moments ar-

rangements calculated self consistently for different values of λ_η . Here, $\lambda_\eta = \eta\lambda$ where λ is the calculated value of SOC strength, for each Mn and W atom, used in determining the results depicted in Fig. 4. We note that the

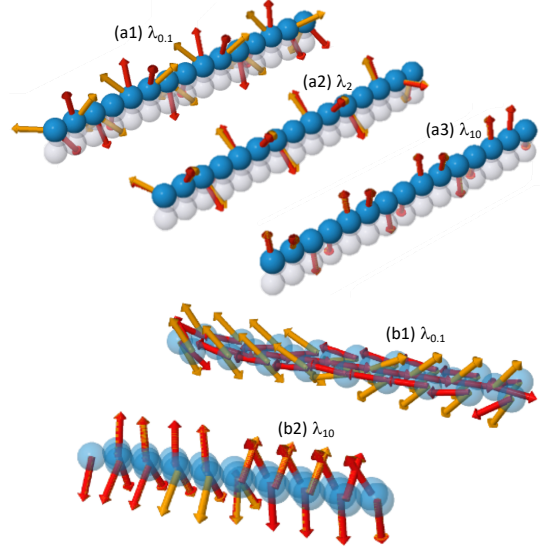


FIG. 5. (Color online) The spin and the orbital magnetic configurations for Mn nanowire (NW) on a W(110) surface for several spin-orbit coupling values λ_η , where $\eta = 1$ refers to 100% of the true SOC value, and *e.g.* $\eta = 0.1$ one tenth of this value. (a1)-(a3): Mn nanowire (NW) with $\eta = 0.1, 2$ and 10 , respectively. (b1)-(b2): Stripe1 for $\eta = 0.1$ and 10 . Yellow (red) arrows denote the spin (orbital) moment directions.

SOC strength has a significant influence on the orientation dependence of the orbital magnetic orderings as well as the magnitude of the Mn orbital moments. The latter tends to increase with the enhancement of the SOC coupling values, with values ranging from $\approx 0.02\mu_B/\text{atom}$, for $\eta = 0.1$, to $\approx 0.6\mu_B/\text{atom}$ for $\eta = 2$. For relatively small values of λ_η the spin and orbital moments of each Mn atom are virtually uncoupled, whereas for sufficiently large SOC values they tend to align in the same direction, as expected.

In order to consider a concrete microscopic Hamiltonian, we have considered the following model:

$$\hat{H} = - \sum_{i \neq j} J_{ij} \hat{S}_i \cdot \hat{S}_j - \lambda \sum_i \hat{L}_i \cdot \hat{S}_i - \hat{H}_{\text{CF}}^{(i)}, \quad (1)$$

where J_{ij} denote the effective Heisenberg (isotropic) exchange interactions between magnetic moments located on sites i and j , \hat{S}_i and \hat{L}_i represent the spin and orbital angular momentum operators, respectively, and λ is the spin-orbit coupling constant. $\hat{H}_{\text{CF}}^{(i)}$ symbolizes the crystal field Hamiltonian.

From the point of view of a more general approach [9] this means that we neglect orbital-orbital and spin-orbital interactions at different sites but take them into

account explicitly at the same site. The intrasite orbital-orbital interaction is nothing but the crystal-field splitting term, as is clear from Stevens operator-equivalent method in the crystal-field theory [45]. Neglecting orbital-related *intersite* interactions is justified by the smallness of orbital magnetic momenta.

For simplicity we shall neglect the explicit presence of the substrate and deal with an ideal atomic wire, characterized by $C_{\infty v}$ point group symmetry. The leading term in the expansion of the crystal field potential for $C_{\infty v}$ symmetry has the form (see e.g.[46]):

$$\hat{H}_{\text{CF}}^{(i)} = V_{\text{CF}}(3\hat{L}_{i,z}^2 - \hat{L}_i^2). \quad (2)$$

Here, we assume that the wire is in z direction. Depending on the sign of V_{CF} , the wire will have easy axis or easy plane for orbital magnetic moments.

According to the model (1), the long-range order character of the spin interactions is primarily defined by the values of the interatomic exchange constants J_{ij} . In the Mn chains, for example, the ground state spin spiral configuration results from competing interatomic interactions. At the same time, the orbital moment on each atom experiences a combined effect of spin-orbit coupling, which tends to align it parallel to the spin moment, and the crystal field that tends to line it up along the orbital easy-axis (or easy plane) [47]. Thus, the final direction of local orbital angular moment \vec{L} depends upon the relative strength of these two terms. In what follows we shall show that this simple model captures the main effects observed in our non-collinear DFT calculations.

The model, defined by Eqs.(1) and (2) was solved for a finite-size chain of spins. We considered a chain of 20 sites with both spin and orbital moments treated as classical vectors of unitary length. Since we aimed at describing $3d$ system, we assume that the J_{ij} 's are much larger than λ . Thus, the spin configuration is primarily defined by the exchange interactions. Restricting the number of inter-site interactions to nearest (J_1) and next-nearest neighbours (J_2), the ground state spin configuration is defined by the maximum of the Fourier transformed exchange interaction:

$$J(q) = 2J_1 \cos(qza) + 2J_2 \cos(2qza), \quad (3)$$

where q is the wavevector of the spiral and a is the inter atomic distance.

For our simulations, we set $J_1=1$ (ferromagnetic) and $J_2=-1$ (antiferromagnetic), which resulted in the cycloidal spiral ground state with wavevector $q_{\text{GS}}=0.21 \times \frac{2\pi}{a}$. The parameters λ and V_{CF} were both positive and their ratio was varied. The summary of the results is shown in Fig. 6. One can see that in the regime when $V_{\text{CF}} < \lambda$, spin and orbital moments are nearly parallel to each other. As V_{CF} is increasing, the distribution over the $\theta(= \angle(\vec{L}_i, \vec{S}_i))$ angles gets broader, indicating that the orbital moments tend to align more and more

along the easy axis direction of the magnetization. Finally, for large V_{CF} , the directions of the orbital moments become locked and each of L_i 's is oriented parallel or antiparallel to z axis, depending on the sign of the $S_{i,z}$ component.

CONCLUSION

In this work we have explored the magnetism of Mn chains of various width (1 - 3 atomic layers) on a W (011) substrate, using a real space electronic structure method. We find that the spin-moments of all investigated systems align in a non-collinear way. This is the result of antiferromagnetic nearest neighbour interactions, coupled to ferromagnetic interactions of longer range. The orbital magnetism is induced via spin-orbit effects, and we have found that spin- and orbital moments of a given Mn atom can exhibit a rather large angle between them, and that the period of the two spin-structures can be distinctly different. The magnetic chirality of spin- and orbital moments is discussed in the light of a microscopic theory that involves Heisenberg exchange, spin-orbit coupling and crystalline electric field. Such competitions have been discussed before for bulk materials [48, 49]. Mn on W(011) represent one more example of such exotic couplings, and that they are fully possible also in nano-sized objects.

ACKNOWLEDGEMENTS

M. M. B-N., R. B. M. and A. B. K. acknowledge financial support from CAPES and CNPq, Brazil. The calculations were performed at the computational facilities of the National Laboratory for Scientific Computing (SDumont, LNCC/MCTI) and CENAPAD, Brazil. O.E. acknowledges support from the Swedish Research Council (VR), the Knut and Alice Wallenberg Foundation, the Swedish Foundation for Strategic Research (SSF), the Swedish Energy Agency (Energimyndigheten), ERC (synergy grant FASTCORR, project 854843), eSENCE, and STandUPP. M.I.K. acknowledges support from ERC (synergy grant FASTCORR, project 854843). The work of Y.K. is supported by VR under the project No. 2019-03569.

-
- [1] A. Fert, V. Cros, and J. Sampaio, Nat. Nanotechnol. **8**, 152 (2013).
 - [2] N. Romming, C. Hanneken, M. Menzel, J. E. Bickel, B. Wolter, K. von Bergmann, A. Kubetzka, and R. Wiesendanger, Science **341**, 636 (2013).

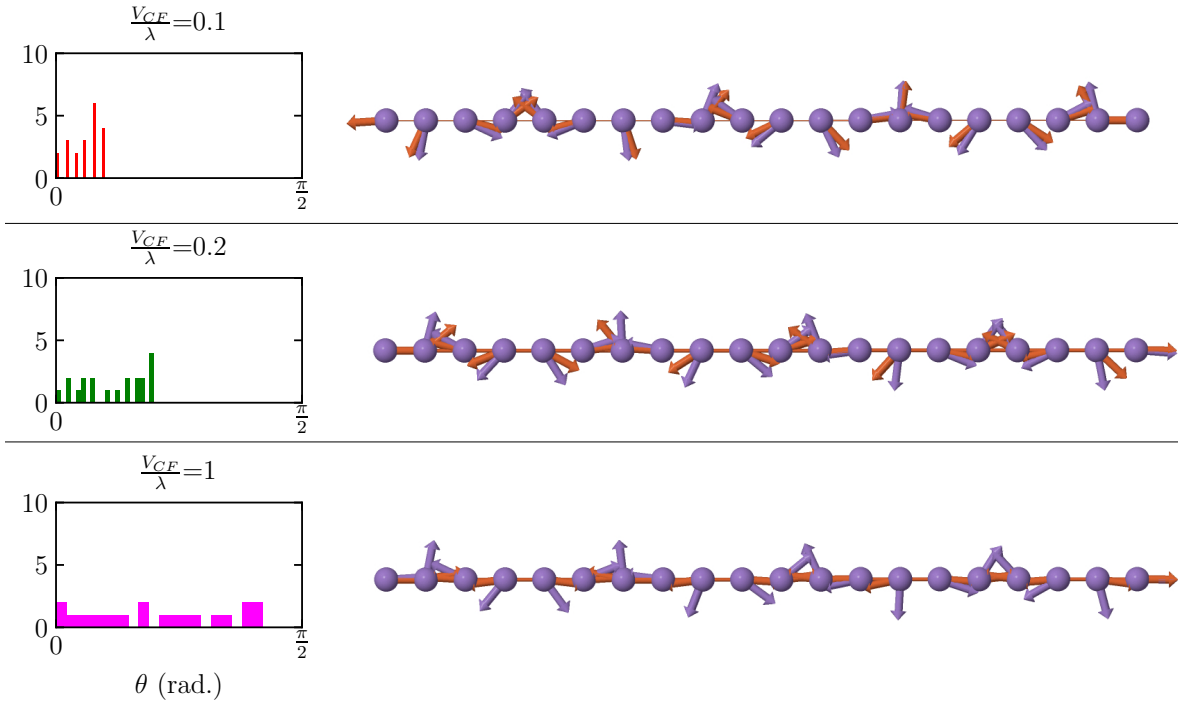


FIG. 6. Left: Histogram of the obtained distribution of the angles (θ) between spin and orbital moments at each site. Right: The ground state magnetic order. Spin (orbital) moments are shown at violet (orange) arrows. Z axis is along the direction of the wire.

- [3] Y. Yoshida, S. Schröder, P. Ferriani, D. Serrate, A. Kubetzka, K. von Bergmann, S. Heinze, and R. Wiesendanger, *Phys. Rev. Lett.* **108**, 087205 (2012).
- [4] M. Bode, M. Heide, K. Von Bergmann, P. Ferriani, S. Heinze, G. Bihlmayer, A. Kubetzka, O. Pietzsch, S. Blügel, and R. Wiesendanger, *Nature* **447**, 190 (2007).
- [5] M. Menzel, Y. Mokrousov, R. Wieser, J. E. Bickel, E. Vedmedenko, S. Blügel, S. Heinze, K. von Bergmann, A. Kubetzka, and R. Wiesendanger, *Phys. Rev. Lett.* **108**, 197204 (2012).
- [6] M. Steinbrecher, R. Rausch, K. T. That, J. Hermenau, A. A. Khajetoorians, M. Pothoff, R. Wiesendanger, and J. Wiebe, *Nat. Commun.* **9**, 1 (2018).
- [7] I. Dzyaloshinsky, *Journal of Physics and Chemistry of Solids* **4**, 241 (1958).
- [8] T. Moriya, *Phys. Rev.* **120**, 91 (1960).
- [9] A. Secchi, A. Lichtenstein, and M. Katsnelson, *Annals of Physics* **360**, 61 (2015).
- [10] S. Mankovsky, S. Polesya, and H. Ebert, *Phys. Rev. B* **101**, 174401 (2020).
- [11] A. Lászlóffy, L. Rózsa, K. Palotás, L. Udvardi, and L. Szunyogh, *Phys. Rev. B* **99**, 184430 (2019).
- [12] S. Grytsiuk, J.-P. Hanke, M. Hoffmann, J. Bouaziz, O. Gomonay, G. Bihlmayer, S. Lounis, Y. Mokrousov, and S. Blügel, *Nat. Commun.* **11**, 1 (2020).
- [13] R. Cardias, A. Bergman, A. Szilva, Y. O. Kvashnin, J. Fransson, A. B. Klautau, O. Eriksson, and L. Nordström, *arXiv:2003.04680 [cond-mat]* (2020), arXiv:2003.04680 [cond-mat].
- [14] T. Tanaka, H. Kontani, M. Naito, T. Naito, D. S. Hirashima, K. Yamada, and J. Inoue, *Phys. Rev. B* **77**, 165117 (2008).
- [15] H. Kontani, T. Tanaka, D. S. Hirashima, K. Yamada, and J. Inoue, *Phys. Rev. Lett.* **102**, 016601 (2009).
- [16] D. Go, D. Jo, C. Kim, and H.-W. Lee, *Phys. Rev. Lett.* **121**, 086602 (2018).
- [17] R. R. Neumann, A. Mook, J. Henk, and I. Mertig, *Phys. Rev. Lett.* **125**, 117209 (2020).
- [18] D. Go and H.-W. Lee, *Phys. Rev. Research* **2**, 013177 (2020).
- [19] S. R. Park, C. H. Kim, J. Yu, J. H. Han, and C. Kim, *Phys. Rev. Lett.* **107**, 156803 (2011).
- [20] J.-H. Park, C. H. Kim, H.-W. Lee, and J. H. Han, *Phys. Rev. B* **87**, 041301(R) (2013).
- [21] S. Kim, K. Ueda, G. Go, P.-H. Jang, K.-J. Lee, A. Belabbes, A. Manchon, M. Suzuki, Y. Kotani, T. Nakamura, *et al.*, *Nat. Commun.* **9**, 1 (2018).
- [22] A. I. Liechtenstein, M. I. Katsnelson, V. P. Antropov, and V. A. Gubanov, *J. Magn. Magn. Mater.* **67**, 65 (1987).
- [23] M. I. Katsnelson and A. I. Lichtenstein, *Phys. Rev. B* **61**, 8906 (2000).
- [24] L. V. Pourovskii, *Phys. Rev. B* **94**, 115117 (2016).
- [25] S. Frota-Pessôa, *Phys. Rev. B* **46**, 14570 (1992).
- [26] A. B. Klautau and S. Frota-Pessôa, *Surf. Sci.* **579**, 27 (2005).
- [27] A. Bergman, L. Nordström, A. B. Klautau, S. Frota-Pessôa, and O. Eriksson, *Phys. Rev. B* **73**, 174434 (2006).
- [28] A. Bergman, L. Nordström, A. Burlamaqui Klautau, S. Frota-Pessôa, and O. Eriksson, *Phys. Rev. B* **75**, 224425 (2007).
- [29] M. M. Bezerra-Neto, M. S. Ribeiro, B. Sanyal, A. Bergman, R. B. Muniz, O. Eriksson, and A. B. Klau-

- tau, Sci. Rep. **3**, 3054 (2013).
- [30] A. B. Klautau and S. Frota-Pessôa, Phys. Rev. B **70**, 193407 (2004).
 - [31] S. Frota-Pessôa, A. B. Klautau, and S. B. Legoas, Phys. Rev. B **66**, 132416 (2002).
 - [32] A. Bergman, L. Nordström, A. B. Klautau, S. Frota-Pessôa, and O. Eriksson, Surface Science **600**, 4838 (2006).
 - [33] R. N. Igarashi, A. B. Klautau, R. B. Muniz, B. Sanyal, and H. M. Petrilli, Phys. Rev. B **85**, 014436 (2012).
 - [34] R. Cardias, M. M. Bezerra-Neto, M. S. Ribeiro, A. Bergman, A. Szilva, O. Eriksson, and A. B. Klautau, Phys. Rev. B **93**, 014438 (2016).
 - [35] R. Cardias, A. Szilva, M. Bezerra-Neto, M. Ribeiro, A. Bergman, Y. O. Kvashnin, J. Fransson, A. Klautau, O. Eriksson, and L. Nordström, Sci. Rep. **10**, 1 (2020).
 - [36] O. K. Andersen, Phys. Rev. B **12**, 3060 (1975).
 - [37] R. Haydock (Academic Press, 1980) pp. 215–294.
 - [38] U. von Barth and L. Hedin, J. Phys. C: Solid State Phys. **5**, 1629 (1972).
 - [39] O. Eriksson, B. Johansson, R. C. Albers, A. M. Boring, and M. S. S. Brooks, Phys. Rev. B **42**, 2707 (1990).
 - [40] S. Frota-Pessôa, Phys. Rev. B **69**, 104401 (2004).
 - [41] N. Beer and D. Pettifor, in *The Electronic Structure of Complex Systems* (Springer, 1984) pp. 769–777.
 - [42] S. Frota-Pessôa, R. B. Muniz, and J. Kudrnovský, Phys. Rev. B **62**, 5293 (2000).
 - [43] A. Szilva, M. Costa, A. Bergman, L. Szunyogh, L. Nordström, and O. Eriksson, Phys. Rev. Lett. **111**, 127204 (2013).
 - [44] A. Szilva, D. Thonig, P. F. Bessarab, Y. O. Kvashnin, D. C. M. Rodrigues, R. Cardias, M. Pereiro, L. Nordström, A. Bergman, A. B. Klautau, and O. Eriksson, Phys. Rev. B **96**, 144413 (2017).
 - [45] K. W. H. Stevens, Proc. Phys. Soc. A (London) **65**, 209 (1952).
 - [46] J. Mulak and Z. Gajek, in *The Effective Crystal Field Potential*, edited by J. Mulak and Z. Gajek (Elsevier Science Ltd, Oxford, 2000) pp. 53 – 63.
 - [47] G. van der Laan, J. Phys.: Condens. Matter **13**, 11149 (2001).
 - [48] S. A. Nikolaev and I. V. Solovyev, Phys. Rev. B **89**, 064428 (2014).
 - [49] O. Grånäs, I. Di Marco, O. Eriksson, L. Nordström, and C. Eitz, Phys. Rev. B **90**, 165130 (2014).